Dendrite fragmentation in alloy solidification due to sidearm pinch-off

H. Neumann-Heyme, K. Eckert, and C. Beckermann

Phys. Rev. E **92**, 060401 — Published 7 December 2015

DOI: 10.1103/PhysRevE.92.060401

Dendrite fragmentation in alloy solidification due to sidearm pinch-off

H. Neumann-Heyme* and K. Eckert
Institute for Fluid Dynamics, Technische Universität Dresden, 01062 Dresden, Germany

C. Beckermann
Department of Mechanical and Industrial Engineering, The University of Iowa, Iowa City, IA 52242, USA

Dendrite sidebranch detachment is an important fragmentation mechanism during solidification of alloys. The detachment occurs at the junction between a sidearm and its parent stem. While this pinching process is driven by capillarity, the presence of solidification opposes the instability. Using a simple numerical model of a single sidearm, we are able to capture the essential dynamics of dendrite sidebranch development and the resulting morphological transitions. While shortly before pinch-off the neck itself obeys well-known universal scaling relations, the overall evolution of the sidearm shape sensitively depends on its initial geometry and the rate of solidification. It is found that pinch-off only occurs over limited ranges of geometrical parameters and cooling rates and is generally bounded by sidearm retraction and coalescence regimes. Simple scaling relations are identified that provide the bounds for the pinch-off regime. Pinching at the branching point is shown to be faster than the Rayleigh-Plateau instability of an infinitely long cylinder.

PACS numbers: 81.10.Aj, 81.30.Fb, 05.70.Ln, 64.70.dg

Fragmentation of dendrites is one of the major unresolved questions in the field of solidification. The detachment of dendrite sidebranches from a larger stem or the breakup of dendrite arms are considered key mechanisms in the formation of grain structure transitions (columnar to equiaxed) in metal alloy castings [1, 2], grain defects such as freckles in single crystal components [1], and highly refined grain structures in solidification of undercooled melts [3, 4]. Despite its technological importance, a systematic understanding of dendrite fragmentation has been difficult to obtain due to the complexity of the processes involved and the challenges associated with its direct experimental observation. Sidebranch detachment has first been noted in experiments with transparent alloys [1] (Fig. 1a). Directional solidification experiments have linked its occurrence to certain transient conditions [1, 5, 6]. More recently, sidebranch detachment events have been observed in metal alloys using synchrotron and X-ray facilities [7–10].

Dendritic structures are characterized by a complex network of primary, secondary and higher order branches (Fig. 1a). After their initial growth in an undercooled melt, the branches undergo a slower evolution near equilibrium that involves both further solidification and capillary driven coarsening. For this later stage, experimental observations have revealed three different scenarios for fundamental changes in the sidebranch morphology [11, 12]: (i) *retraction* of small sidebranches towards their parent stem (Fig. 1a, red selection), (ii) *pinch-off* or detachment of sidebranches at the narrow neck with the parent stem (Fig. 1a, yellow selection), and (iii) *coalescence* of neighbouring sidebranches. In the present study,

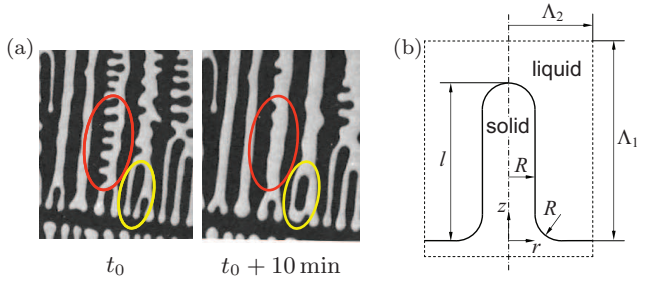

FIG. 1. (Color online) (a) Sidebranch evolution as shown in the classical experiments by Jackson & Hunt [1] (black: solid): retraction (red) and fragmentation (yellow). (b) Axisymmetric sidearm model and parameters of the initial geometry.

pinch-off of sidebranches is investigated as a cause of dendrite fragmentation. It will be seen that retraction and coalescence bound the pinch-off regime to a rather limited parameter range.

Capillary driven pinching occurs in numerous two-phase systems. Elongated interface shapes are prone to a pinching instability that results from a minimization of surface energy, with mass or heat transport occurring through the interior and/or the embedding phase. Examples can be found in hydrodynamics [13, 14], material sciences [15–17], nanotechnology [18], and biology [19, 20]. The final stage of pinching, when the neck radius approaches zero, is characterized by strong localization and acceleration of the neck dynamics, leading to self-similar, universal behaviour. Recently, this phenomenon has been analyzed in coarsening of metallic alloys [16, 17].

One well-known pinching mechanism is the Rayleigh-Plateau instability (RPI) of an infinitely long, perturbed cylindrical rod subject to capillarity. The RPI has been used to explain grain refinement in solidification of un-

* hieram.neumann-heyme@tu-dresden.de

dercooled melts [3, 4]. Here, the sidebranches are assumed to be already detached from the primary dendrite trunks, and the RPI then acts on the remaining corrugated trunks to produce fragments. While this mechanism can indeed be responsible for the grain refined, fully equiaxed microstructures that are observed in solidification of undercooled droplets, the present study focuses on the initial sidebranch detachment process during columnar growth. In solidification of castings, the primary trunks in the columnar zone usually do not fragment, but dendrite sidearms can still detach and become equiaxed grains [1, 2]. All previous direct experimental observations [1, 5–9] confirm this mechanism and reveal that the location for the pinch-off is the narrow neck that naturally develops close to the junction between a sidebranch and its parent stem (Fig. 1a).

Previous capillary pinching theories [4, 15, 17] are limited to isothermal conditions. However, alloy solidification processes such as metal casting involve a continuous decrease in temperature, such that the overall fraction of solid in the system increases. In the present study, the pinching dynamics are investigated in the presence of cooling and net solidification. Whereas capillarity results in a continual decrease in the neck radius during pinching, solidification tends to increase the radius of the neck.

The majority of the pinching process takes place in a nonlinear regime that is neither accessible to a linear stability analysis nor to a self-similar description. Here, we introduce a numerical model of concurrent growth and coarsening of a simplified dendritic structure of a solidifying binary alloy. It allows for quantitative predictions of characteristic durations and parameter regimes for pinch-off, retraction, and coalescence of dendrite sidearms. The model considers a generic axisymmetric sidearm, connected at a right angle to a larger parent stem. The initial geometry of the sidearm, Fig. 1b, is given by a cylinder of radius R and length l that is attached to a planar base. The sidearm tip and root sections are circularly rounded. The sidearm and its base are contained in a domain of longitudinal and radial dimensions of Λ_1 and Λ_2, respectively, which can be thought of as half of the primary and secondary dendrite arm spacings. The sidearm dimensions relative to the domain size determine the initial fraction of solid in the system. The initial solute concentrations in the liquid and solid are c_l^0 and kc_l^0, respectively, corresponding to phase equilibrium at the initial temperature $T = T_0$, where k is the partition coefficient. The domain is sufficiently small that it can be assumed to be at a uniform temperature T. This temperature decreases over time with a specified constant cooling rate $\dot{T}$. The constant cooling rate assumption is commonly made in modeling of directional (columnar) solidification. Diffusion of solute in the melt (diffusion of solute in solid is neglected), expressed as a scaled supersaturation $U = (c - c_l^0)/\Delta c_0$, and the dynamics of the solid-liquid interface are governed by:

$$\partial_t U = D\nabla^2 U \tag{1}$$

$$[1 + (1-k)U|_i]\, V_n = -D\partial_n U|_i^+ \tag{2}$$

$$U|_i = -d_0\kappa + \theta, \tag{3}$$

where $\theta = (T_0 - T)/|m|\Delta c_0$ is the dimensionless temperature scaled by the equilibrium concentration gap $\Delta c_0 = c_l^0(1-k)$, and t is time. D, m, V_n, and κ refer to the solute diffusivity in the melt, liquidus slope, normal interface velocity, and sum of the principal curvatures of the solid-liquid interface, respectively. The normal vector n is oriented towards the liquid phase. $d_0 = \Gamma/|m|\Delta c_0$ is the chemical capillary length, with Γ being the Gibbs-Thomson coefficient. The subscript i and superscript $+$ denote the interface location and positive normal direction, respectively. In order to represent a periodic array of equally spaced and sized sidearms, no-flux conditions are applied on all domain boundaries.

Additional insight can be gained by introducing the following dimensionless length and time and change of variables for the supersaturation

$$\widetilde{r} = r/R, \qquad \widetilde{t} = tDd_0/R^3, \qquad \widetilde{U} = (U-\theta)R/d_0. \tag{4}$$

Herein, the initial sidearm radius R is taken as the characteristic length and (without restrictions) $R \propto t^{1/3}$ is acknowledged as an intrinsic scaling for coarsening dynamics [16, 21]. Since the initial growth of a sidearm is not considered, $d_0/R \ll 1$ is generally true. Introducing the dimensionless variables of Eq. (4) into Eqs. (1-3) and letting $d_0/R \to 0$, yields

$$\dot{\theta} = \nabla^2 U \tag{5}$$

$$[1 + (1-k)\theta]\, V_n = -\partial_n U|_i^+ \tag{6}$$

$$U|_i = -\kappa. \tag{7}$$

Here, and in the following, the tilde is omitted for convenience, and $\dot{\theta} = -\dot{T}R^3/D\Gamma$ is the scaled cooling rate. We verify in Ref. [22] that Eqs. (5-7) are accurate for $d_0/R \lesssim 10^{-4}$. This limit is satisfied for all sidearm radii encountered in common solidification processes and implies that the interface dynamics are slow compared to the relaxation of the diffusion field. As Eq. (5) shows, solute diffusion can then be treated as quasi-stationary. Note that the scaled problem is independent of D, d_0, and R. For vanishing cooling rates $\dot{\theta} = \theta = 0$, corresponding to isothermal coarsening, the sidearm evolution is determined entirely by geometrical parameters. In the presence of solidification ($\dot{\theta} > 0$), the partition coefficient k remains as the only material parameter and is taken as $k = 0.14$ (Al-Cu) for illustrative purposes, unless mentioned otherwise.

For the numerical implementation of the present problem, Eqs. (5-7) were reformulated as a phase-field model [22, 23] in axisymmetric form. The phase-field model was solved by an adaptive finite element code with semi-implicit time integration [24]. A detailed study was performed to verify that the present results are independent

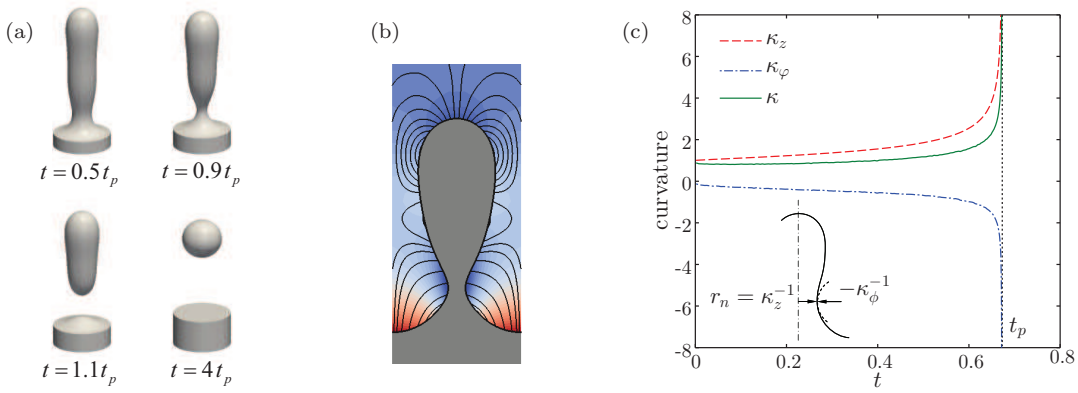

FIG. 2. (Color online) (a) Time evolution of the arm shape. (b) Flux lines of the diffusive transport during isothermal coarsening; solute concentration: high (red), low (blue). (c) Curvature components and total curvature during pinching as a function of time.

of the diffuse interface thickness and other computational parameters used in the phase-field model [22]. In addition, the calculated variation of the neck radius near pinch-off is compared below to an exact analytical solution and excellent agreement is obtained.

Figure 2a shows an example of the computed evolution of the sidearm shape during a pinching process. Time is measured relative to the pinch-off time t_p. In this example, the cooling rate is zero and interface motion is driven purely by diffusive mass exchange between interface regions of different curvatures due to the Gibbs-Thomson effect, Eq. (3). Solid tends to melt in regions of higher curvature and accumulate in regions of lower curvature. Mass exchange and interface motion is generally promoted by either high curvature contrasts or short diffusion paths. The diffusion processes can be visualized well by the flux lines [25, 26] plotted in Fig. 2b. Within a short time from the start of the simulation, a narrow neck is formed immediately above the junction between the sidearm and the parent stem. This can be attributed to the short diffusion paths between the stem and the sidearm in this region. The tip of the sidearm retracts due to its high curvature and the sidearm evolves into a more evenly rounded shape. Later, the sidearm pinches off at the neck and the resulting fragment coarsens into a sphere.

The evolution of the neck in the region where the pinch-off occurs is controlled by the local curvature components. The computed variations of the circumferential curvature $\kappa_z = r_n^{-1}$, where r_n is the minimum neck radius, and the meridional curvature κ_φ, together with their sum κ, are plotted in Fig. 2c. While κ_z is always positive and promotes melting and pinch-off, the negative κ_φ counteracts this effect. During most of the coarsening process, the magnitudes of κ_z and κ_φ increase slightly, while the sum of the two curvatures κ, remains almost constant and close to unity. Within a short period before pinch-off, κ_z becomes suddenly dominant and the neck collapses. These curvature evolutions demonstrate that the final stage of the pinching process is very fast and localized.

This localized behaviour has recently led to the development of a general theory of curvature-driven pinching dynamics in the presence of external volume diffusion [17]. The theory shows that the pinching region eventually acquires a self-similar shape that approaches a double cone with an angle of 80°. During this stage, the neck radius varies as $r_n(t) = 0.88(t - t_p)^{1/3}$. Figure 3a shows that the present results for the variation of the neck radius and the shape of the neck at pinch-off (inset) indeed approach the theoretical predictions of Ref. [17]. This agreement lends not only confidence to the present computations but also provides additional insight into the universality of the theory. Included in Fig. 3a are results not only for purely curvature-driven pinching, but also for two finite cooling rates. As expected, in the presence of net solidification the neck radius approaches zero more slowly and the neck shape is generally wider. However, the very last stage of pinching is still characterized by the same universal dynamics as predicted by the theory, which was originally developed for isothermal conditions. This indicates that the localized nature of the pinch-off process effectively eliminates any influence of the global geometry and even opposing effects such as solidification. Nonetheless, the theory of Ref. [17] is limited to a very short time interval before pinch-off, and it cannot provide a full understanding of the entire sidearm pinching process during solidification.

The effect of the competition between solidification and coarsening on dendrite fragmentation is now demonstrated for a typical initial sidearm geometry by varying the cooling rate. Figure 3b shows the times obtained for certain events to occur, together with the associated sidearm shapes. At low cooling rates, including negative values, the sidearm retracts towards the primary stem because remelting of the tip takes less time than remelting of the neck. Although the time to retraction increases with increasing cooling rate, coarsening dominates over

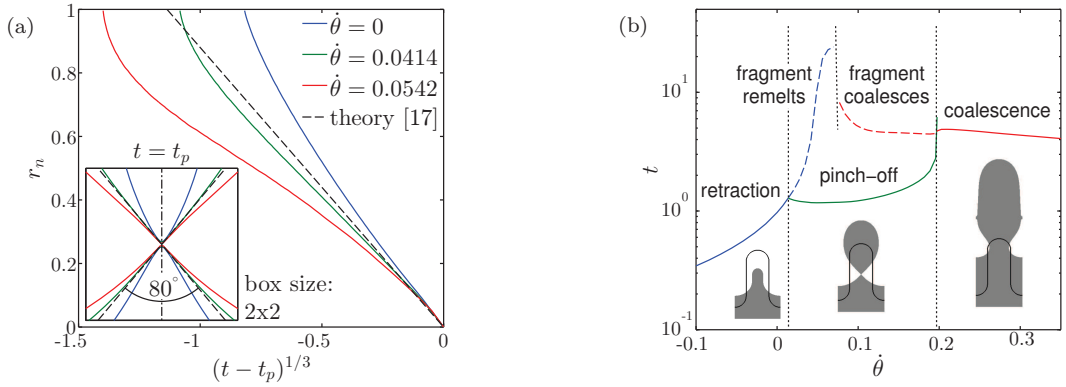

FIG. 3. (Color online) (a) Evolution of the neck radius r_n, and interface shape at pinch-off (inset) for three cooling rates and comparison with the theory of Ref. [17]. (b) Durations of the different sidearm evolution scenarios as a function of cooling rate ($\Lambda_2 = 2$, $l = 5$, $\Lambda_1 = 15$); dashed lines refer to the fragment itself.

solidification in this regime. At high cooling rates, the lateral growth of the sidearm above the neck is so rapid that it coalesces with a neighboring arm before any pinch-off can occur. The pinch-off regime is limited to a relatively small range of intermediate cooling rates. The time to fragmentation increases slightly with increasing cooling rate, reflecting the fact that solidification opposes the curvature-driven necking process. The resulting fragment experiences either remelting or coalescence, with the transition between the two being characterized by a spherical fragment where solidification exactly balances remelting due to the Gibbs-Thomson effect.

A more general characterization of the durations and parameter ranges identified in Fig. 3b can be obtained by analyzing some important limiting cases consisting of (i) the isothermal limit ($\dot\theta = 0$), where the fraction of solid in the system remains constant and Λ_1 has no influence, and (ii) the limit of a long sidearm, where interactions between the tip and neck regions are negligible.

Long arm, isothermal: In this most elementary case, Λ_2 is the only relevant parameter. With increasing Λ_2 the pinch-off time rapidly decreases towards an asymptotic value of $t_p(\Lambda_2 \to \infty) = 0.52$ [22]. It is interesting to note that this equation, rewritten in dimensional form, is the same as Eq. (4) in [3] for the breakup time of an infinitely long rod undergoing a RPI, except that the constant in [3] is equal to 3/2. We performed additional phase-field simulations for an infinitely long rod and found that a perturbation at the fastest growing wavelength and with an amplitude of $0.1R$ gives a breakup time that is about four times larger than the value of 0.52 for a branched shape. Hence, even for long sidearms where the RPI could become an issue, dendrite fragmentation is more likely to occur by pinching near the branching point.

Finite arm, isothermal: This case characterizes the competition between retraction and pinching at low arm lengths. Figure 4a shows the critical arm length $l_{r\text{-}p}$ as a function of Λ_2 above which a sidearm pinches off rather than retracts (see Fig. 1a). The critical arm length increases with a larger sidearm spacing because the diffusive flux between the retracting tip and the root region is less restricted, and $l_{r\text{-}p}$ rapidly approaches an upper limit of 6.67. This limit for the isothermal case also provides the upper arm length limit for retraction in a solidifying system ($\dot\theta > 0$), because sidearm growth only reduces $l_{r\text{-}p}$.

Long arm, varying cooling rate: Under non-isothermal conditions, remelting due to high curvatures is opposed by progressive solidification. Therefore, both retraction and pinch-off are delayed or do not occur at all. Here, we investigate the effect of this competition on the evolution of the neck in the long sidearm limit. The inset in Fig. 4b indicates that for a given Λ_2, the pinch-off time increases with cooling rate and tends to infinity at a critical value of the cooling rate $\dot\theta_{p\text{-}c}$, where curvature- and solidification-induced effects at the neck are exactly balanced. At higher cooling rates, the neck radius remains finite, no pinch-off occurs, and the sidearm eventually coalesces with its neighbour. The two curves in the inset of Fig. 4b show that a larger Λ_2 results in a smaller critical cooling rate $\dot\theta_{p\text{-}c}$, for the pinch-off to coalescence transition. This indicates that solidification effects are stronger for large Λ_2 and, hence, low fractions of solid in the system. The fact that solidification rates are higher at low solid fractions can be inferred from the Scheil equation [27]. At infinitely large spacings, the critical cooling rate for the pinch-off to coalescence transition reaches a lower bound of $\dot\theta_{p\text{-}c} = 0.023$ ($k = 0.5$). This value is a general upper limit for the cooling rate up to which pinch-off is possible. Also note from Fig. 4b that the partition coefficient k has only a small effect on $\dot\theta_{p\text{-}c}(\Lambda_2)$. At early times, k plays a negligible role due to a small θ in Eq. (6). During the final stage, when the neck region approaches universal behaviour (Fig. 3a), the influence of k vanishes again. The fact that pinch-off is generally favoured by low spacings between the sidearms is a further interesting outcome of the results in Fig. 4. Low Λ_2 increase both the sidearm length range, Fig. 4a, and the cooling

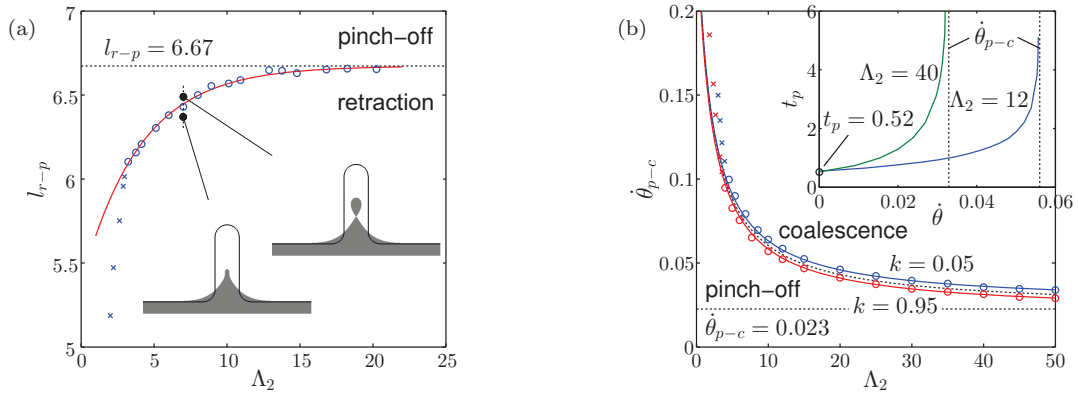

FIG. 4. (Color online) (a) Critical sidearm length for the retraction to pinch-off transition as a function of the spacing Λ_2 for isothermal coarsening; fitted by $l_{r\text{-}p}(\Lambda_2) = [6.67 - 1.3\exp(-0.25\Lambda_2)]$. (b) Long sidearm limit: pinch-off time versus cooling rate (inset) and dependence of the critical cooling rate for the pinch-off to coalescence transition on Λ_2 for different k; fitted by $\dot{\theta}_{p\text{-}c}(\Lambda_2, k) = 0.446/(\Lambda_2 + 1.86) + 0.0226$ for $k = 0.5$ (dashed line). All data points representing regime boundaries are obtained by an adaptive search scheme in the 2d parameter space. Cross symbols were excluded from fitted data.

rate range, Fig. 4b, over which pinch-off can occur.

Curvature-driven coarsening and net solidification compete in complex and heretofore largely unknown ways in shaping the dendritic microstructure of an alloy. Using a simple axisymmetric model of periodic sidearms, we were able to derive fundamental characteristics and limits of the pinching instability at the junction between a sidearm and its parent stem. Although the neck ultimately converges to a universal self-similar shape at pinch-off, the pinch-off time is a strong function of the initial arm geometry and cooling rate. Pinching at the sidearm junction is shown to be more likely than the RPI of an infinitely long rod. Two important limits have been established, which can be summarized in physical units as follows. A long sidearm will always pinch off if $\dot{T} \gtrsim -0.023 D\Gamma/R^3$. Retraction is only possible if $l/R < 6.67$ (for $\dot{T} \leq 0$). Generally, the tendency for pinch-off is enhanced for smaller Λ_2, i.e. higher initial solid fractions. These relations may provide effective guidance for future experimental and numerical studies on dendrite fragmentation. The effects of more complex non-axisymmetric and non-periodic dendrite arm geometries and of melt convection are deserving of additional research attention.

This work was financially supported by the Helmholtz alliance (LIMTECH) and NASA (NNX14AD69G).

[1] K. Jackson, J. Hunt, D. Uhlmann, and T. Seward, T Metall Soc AIME **236**, 149 (1966).
[2] A. Hellawell, S. Liu, and S. Lu, JOM **49**, 18 (1997).
[3] M. Schwarz, A. Karma, K. Eckler, and D.M. Herlach, Phys Rev Lett **73**, 1380 (1994).
[4] A. Karma, Int J Non-equilib Pr **11**, 201 (1998).
[5] T. Sato, W. Kurz, and K. Ikawa, T Jpn I Met **28**, 1012 (1987).
[6] S. Liu, S. Lu, and A. Hellawell, J Cryst Growth **234**, 740 (2002).
[7] R. H. Mathiesen, L. Arnberg, P. Bleuet, and A. Somogyi, Metall Mater Trans A **37A**, 2515 (2006).
[8] H. Yasuda, Y. Yamamoto, N. Nakatsuka, T. Nagira, M. Yoshiya, A. Sugiyama, I. Ohnaka, K. Umetani, and K. Uesugi, Int J Cast Metal Res **21**, 125 (2008).
[9] H. Jung, N. Mangelinck-Noel, H. Nguyen-Thi, N. Bergeon, B. Billia, A. Buffet, G. Reinhart, T. Schenk, and J. Baruchel, Int J Cast Metal Res **22**, 208 (2009).
[10] E. Liotti, A. Lui, R. Vincent, S. Kumar, Z. Guo, T. Connolley, I. P. Dolbnya, M. Hart, L. Arnberg, R. H. Mathiesen, and P. S. Grant, Acta Mater **70**, 228 (2014).
[11] A. Papapetrou, Z Kristallogr **92**, 89 (1935).
[12] S. Huang and M. Glicksman, Acta Metall Mater **29**, 717 (1981).
[13] J. Eggers, Rev Mod Phys **69**, 865 (1997).
[14] R. Seemann, M. Brinkmann, T. Pfohl, and S. Herminghaus, Rep Prog Phys **75** (2012).
[15] H. Cline, Acta Metall Mater **19**, 481 (1971).
[16] L. K. Aagesen, A. E. Johnson, J. L. Fife, P. W. Voorhees, M. J. Miksis, S. O. Poulsen, E. M. Lauridsen, F. Marone, and M. Stampanoni, Nat Phys **6**, 796 (2010).
[17] L. K. Aagesen, A. E. Johnson, J. L. Fife, P. W. Voorhees, M. J. Miksis, S. O. Poulsen, E. M. Lauridsen, F. Marone, and M. Stampanoni, Acta Mater **59**, 4922 (2011).
[18] S. Karim, M. E. Toimil-Molares, A. G. Balogh, W. Ensinger, T. W. Cornelius, E. U. Khan, and R. Neumann, Nanotechnology **17**, 5954 (2006).
[19] F. Campelo and A. Hernandez-Machado, Phys Rev Lett **100**, 158103 (2008).
[20] E. Hannezo, J. Prost, and J.-F. Joanny, Phys Rev Lett **109**, 018101 (2012).
[21] W. Mullins, J Appl Phys **59**, 1341 (1986).
[22] See Supplemental Material at [URL will be inserted by publisher] for further details on validity of the quasi-stationary approximation; description and convergence of the phase field model; pinch-off time as a function of

spacing for the long arm, isothermal case.
[23] B. Echebarria, R. Folch, A. Karma, and M. Plapp, Phys. Rev. E **70**, 061604 (2004).
[24] A. Voigt and T. Witkowski, J Comput Sci **3**, 420 (2012); T. Witkowski, Ph.D. thesis, Technische Universität Dresden (2013).
[25] S. Marsh and M. Glicksman, Metall Mater Trans A **27**, 557 (1996).
[26] A. Bejan, *Convection Heat Transfer* (Wiley, New York, 1984) Chap. 11.
[27] W. Kurz and D. J. Fisher, *Fundamentals of Solidification* (Trans Tech Publications, 1998).